





Augmented chalcopyrites: A search for new Cu-In-Te phases

Andy Paul Chen ^{*}, Wei Nong , Maung Thway, Jose Recatala-Gomez , and Haiwen Dai 

School of Materials Science and Engineering, Nanyang Technological University, 50 Nanyang Avenue, Singapore 639798, Singapore

Wenhao Zhai  and D. V. Maheswar Repaka 

*Institute of Materials Research and Engineering, Agency for Science, Technology and Research,
2 Fusionopolis Way, Singapore 138634, Singapore*

Kedar Hippalgaonkar[†]

*School of Materials Science and Engineering, Nanyang Technological University, 50 Nanyang Avenue, Singapore 639798, Singapore
and Institute of Materials Research and Engineering, Agency for Science, Technology and Research,
2 Fusionopolis Way, Singapore 138634, Singapore*



(Received 6 March 2024; accepted 1 August 2024; published 26 August 2024)

Chalcopyrites are ternary crystalline compounds which have found use in a diverse array of applications, from solar cells to thermoelectric devices. These are known to be ternary-compound analogs to diamond or sphalerite. “Defect chalcopyrites,” which are chalcopyrite structures stabilized with ordered vacancies and substitutions, are well attested and can serve as a method of tuning material properties through control of stoichiometry. In particular, defect chalcopyrites related to the thermoelectric compound CuInTe_2 comprise a large range of compositions in the pseudobinary system $(\text{Cu}_2\text{Te})_x(\text{In}_2\text{Te}_3)_{1-x}$, where $x < 0.5$. In contrast, the converse case of “augmented chalcopyrites,” namely, $x > 0.5$, is much less known or studied. We report the discovery of a range of Cu_2Te -rich compositions in this binary system where stable phases can potentially be found. Here, the stoichiometry of augmented chalcopyrites is likely to be modulated by the concentration of defect clusters $[\text{Cu}_{\text{In}}^{2-} \cdot 2\text{Cu}^+]^0$ in chalcopyrite CuInTe_2 .

DOI: [10.1103/PhysRevMaterials.8.083801](https://doi.org/10.1103/PhysRevMaterials.8.083801)

I. INTRODUCTION

Copper indium telluride (CuInTe_2) belongs to a class of chalcopyrite compounds, sometimes called diamondlike or adamantine semiconductors, known for exhibiting an interplay of electrical and thermal transport properties resulting in strong thermoelectric functionalities [1,2]. In addition, they have direct electronic band gaps and high optical absorption coefficients, which makes them attractive as photovoltaic materials [3]. Exploring the Cu-In-Te ternary system for erstwhile unknown phases is thus of particular interest for the discovery of new functional materials.

To date, single phases of several compositions have been attested in the Cu-In-Te ternary system: CuIn_5Te_8 [3–6], CuIn_3Te_5 [5–7], $\text{Cu}_2\text{In}_4\text{Te}_7$ [6,8], and $\text{Cu}_3\text{In}_5\text{Te}_9$ [6,9]. A commonality between these compounds is the attestation of their crystal symmetries as chalcopyrite ($I\bar{4}2d$) or cadmium thiogallate ($I\bar{4}$), and also adamantine structures. As such, these compositions are commonly understood as the chalcopyrite CuInTe_2 with the addition of defect species (In_{Cu} , V_{Cu}) as indicated by the elemental composition [2]. As these defects occur in an “ordered and stoichiometric fashion,” they are known as ordered vacancy compounds [10]. Another point

in common is the attested compositions on the pseudobinary system $(\text{Cu}_2\text{Te})_x(\text{In}_2\text{Te}_3)_{1-x}$. This pseudobinary system, which forms a line in the Cu-In-Te ternary phase diagram [Fig. 1(a)], is due to the application of the constraint of the nominal oxidation states of Cu, In, and Te to +1, +3, and –2, respectively, as is the case in CuInTe_2 . As the next most stable phase of Cu-In-Te would likely adopt these same oxidation states, our study is predicated on the supposition that the next most likely new phase in the Cu-In-Te ternary system could lie on this line.

Density functional theory (DFT)-based calculations of formation energy have been widely used to assess the stability of compounds. Formation enthalpies, accessible through DFT calculations at 0 K, have been shown to dominate the stability of materials with up to three chemical components [11]. Accurate assessments of stability for ternary systems require large data sets of DFT-compatible crystal structures, which are found and applied in Materials Project [12] and OQMD [13] databases. Our first-principles approach to materials discovery in the Cu-In-Te system is based on their methods, but also supplemented with several approaches in materials discovery as well as semiempirical formation energy corrections.

While stability serves as a guide to help us eliminate implausible crystal structures from large or randomly generated data sets, synthesizability depends on complex processes of nucleation and crystal growth and the interplay between

^{*}Contact author: andypaul.chen@ntu.edu.sg

[†]Contact author: kedar@ntu.edu.sg

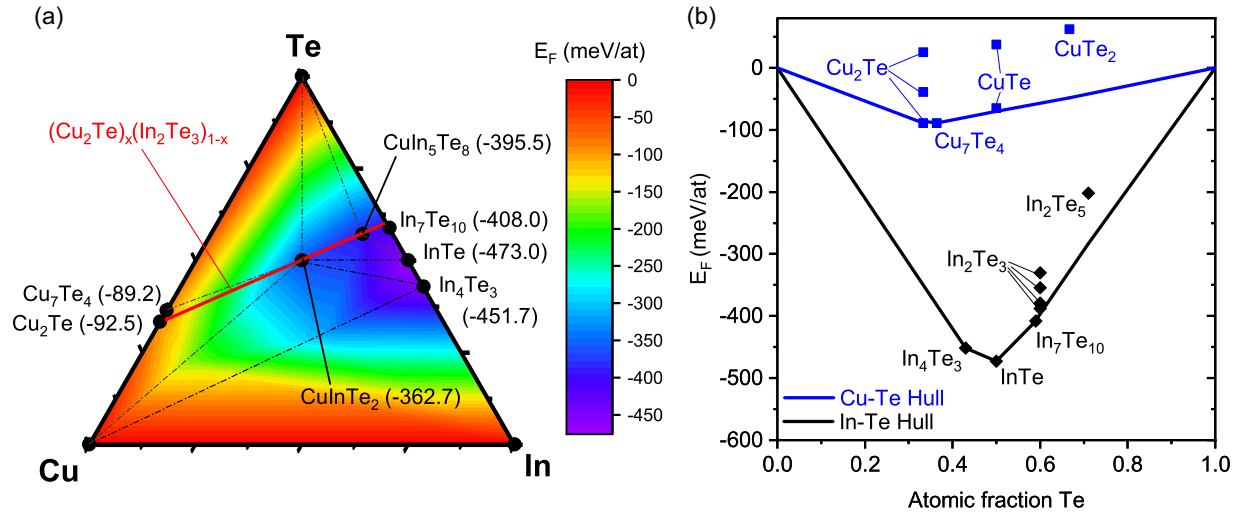


FIG. 1. (a) Convex hull diagram of the formation energy of the Cu-In-Te ternary system. The pseudobinary system $(\text{Cu}_2\text{Te})_x(\text{In}_2\text{Te}_3)_{1-x}$ is marked by the red line. Formation energies of hull phases (in units of meV/atom) are displayed in parentheses. (b) Binary hull diagrams of the In-Te and Cu-Te systems.

reagents, and may not perfectly correlate to thermodynamic stability (see Fig. 1 in Ref. [14]). In this work, we focus chiefly on the thermodynamic stability of phases.

Notation

For Cu-In-Te compounds or any analogous ternary compound referred to in this paper, we adopt the notation $a:b:c$ to represent the stoichiometry of $\text{Cu}_a\text{In}_b\text{Te}_c$. Polymorphs or virtual phases ϕ are represented throughout the paper in abbreviated symbols (in italics). Where applicable, the International Mineralogical Association (IMA-CNMNC) standard notation [15] is used; these are distinguished by the capitalization of their initial letters. Otherwise, a noncapitalized symbol is used instead.

Point defects are denoted using the modified Kröger-Vink notation: for example, in A_B^q , the atom or vacancy A occupies site B to produce a point defect of net charge q .

The coordination number of an atomic species A is denoted by the symbol \mathcal{U}_A . In this work, coordination to different atomic species is distinguished; the coordination of species A to species B is thus denoted by $\mathcal{U}_{A \rightarrow B}$.

II. METHODOLOGY

The formation energy $E_f(\phi)$, of a given solid phase ϕ (comprising any set of vectors completely describing the crystal system and atomic coordinates in Cartesian space), is defined as the difference between the total energy of the phase and the sum of the chemical potentials μ_i of its component atoms, with n_i being the number of atoms of species i present in the system:

$$E_f(\phi) = E_T(\phi) - \sum_i n_i \mu_i. \quad (1)$$

Following the assumption that the solid phase in question is crystalline, all terms of Eq. (1) can be defined in relation to a single unit cell. The chemical potentials μ_{Cu} , μ_{In} , and μ_{Te} are

defined as the energy per atom, respectively, of fcc Cu, bct In, and hexagonal Te.

First-principles calculations are conducted with the Vienna *Ab initio* Simulation Package (VASP) [16–19]. The atomic potentials are modeled by the generalized gradient approximation using the Perdew-Burke-Ernzerhof scheme (GGA-PBE) [20,21]. In all calculations, the plane-wave energy cutoff is set to 600 eV. To account for interactions involving strongly correlated Cu *3d* electrons and to obtain accurate predictions of the conducting or insulating behavior of materials, we adopt the DFT+*U* scheme [22,23] implemented with the method of Dudarev and Botton [24]. The Hubbard parameter $U = 4.0$ eV [25,26] is applied on Cu in electronics structure calculations. In formation energy calculations, we adopt the semiempirical FERRE method of Stevanović *et al.* [27]. This is done by applying the Hubbard parameter $U = 5.0$ eV on Cu in conjunction with adjusting the chemical potentials of Cu, In, and Te by +0.05 eV, +0.41 eV, and –0.11 eV, respectively.

Before each total energy calculation, the structures first undergo a structural relaxation step in which the atomic coordinates, cell volume, and lattice parameters are all relaxed until forces on all atoms fall below 0.05 eV/Å. Next, the total energy is calculated based on the relaxed crystal structure. During both steps, electronic convergence is achieved when the energy change between successive electronic steps falls below 1 meV. Also, a Monkhorst-Pack mesh centered on the Γ point is generated for each structure with the maximum allowed spacing of 0.15 Å⁻¹ to sample the first Brillouin zone of the reciprocal space.

The Cu-In-Te hull is constructed from the formation energies per atom of all crystal structures taken into consideration. The energy above the hull, $\Delta_H E_f$, is a measure of the energy released per atom by the decomposition of a phase to hull phases, and is taken to be roughly inversely correlated to synthesizability. However, the exact prediction of synthesizability goes beyond thermodynamic stability and hence requires a deeper discussion.

TABLE I. Crystal structures by composition in the $(\text{Cu}_2\text{Te})_x(\text{In}_2\text{Te}_3)_{1-x}$ pseudobinary system considered in this study, excluding defect-bearing supercells (see Table II). Formation energies E_F and formation energies above hull, $\Delta_H E_F$, are in units of meV/atom.

Prototype	Name (ϕ)	$\Delta_H E_F$	mp-id [12]/Ref.
In_2Te_3 ($x = 0$)			
In_2Te_3	Zaslavskii <i>et al.</i> (Sp') ^a	41.6	mp-622511 [28]
In_2Te_3	Woolley <i>et al.</i> (Sp'') ^{a,b}	8.0	mp-1223866 [29]
Bi_2Te_3	Tellurobismuthite (<i>Tbi</i>)	66.3	mp-1068510 [30,31]
In_2Se_3	Wurtzite (Wur') ^a	17.1	[32]
CuIn_5Te_8 ($x = 1/6$)			
CuIn_5Te_8	Stannite (Stn') ^a	0	mp-1224528 [4]
CuIn_3Te_5 ($x = 1/4$)			
AgBi_3S_5	Pavonite (<i>Pav</i>)	146.7	mp-23474 [33]
CuIn_3Se_5	Stannite (Stn'') ^a	5.8	mp-1224175 [5–7]
CuInTe_2 ($x = 1/2$)			
CuInTe_2	Chalcopyrite (<i>Ccp</i>)	0	mp-22261 [1,34–36]
Constructed	Wurtzite (Wur'')	54.9	This work
Constructed	Wurtzite (Wur''') ^b	10.8	This work
$\text{Cu}_6\text{In}_4\text{Te}_9$ ($x = 3/5$)			
Constructed	Te-vacancy (tv')	74.2	This work
Constructed	Te-vacancy (tv'')	58.7	This work
$\text{Cu}_4\text{In}_2\text{Te}_5$ ($x = 2/3$)			
Constructed	Quasiantifluorite (afs'')	35.9	This work
Cu_3InTe_3 ($x = 3/4$)			
Cu_3AsS_3 or Cu_3SbS_3	Tetrahedrite (<i>Ttr</i>)	213.9	mp-647606, mp-04884 [37]
Cu_3SbS_3 or Cu_3SbSe_3	Bytzite (<i>Btz</i>)	76.2	mp-24976 [38]
Cu_3BiS_3 or Cu_3SbS_3	Wittichenite (<i>Wtc</i>)	87.5	mp-607291 [39]
Cu_3SbS_3	Skinnerite (<i>Ski</i>)	71.6	mp-554272 [40,41]
Ag_3AsS_3 , Ag_3AsSe_3 , or Ag_3SbS_3	Proustite (<i>Prs</i>)	107.1	mp-24976 [42]
Ag_3SbS_3	Pyrostilpnite (<i>Psti</i>)	130.7	mp-555269 [43]
Ag_3AsS_3	Xanthoconite (<i>Xcn</i>)	90.4	mp-24976 [44]
Ag_3AsSe_3	Kanatzidis and Chou (<i>kc</i>)	137.8	mp-662599 [45]
Constructed	Te-vacancy (tv''')	167.9	This work
Cu_5InTe_4 ($x = 5/6$)			
Ag_5SbS_4	Stephanite (<i>Sph</i>)	93.3	mp-4004
Ag_5BS_4	Thomas (<i>tm</i>)	60.2	mp-1229225 [46]
Ag_5SbSe_4	Yue <i>et al.</i> (<i>yue</i>)	137.3	[47]
Constructed	Quasiantifluorite (afs')	50.6	This work
Cu_2Te ($x = 1$)			
Cu_2Te	Antifluorite (<i>Flr</i>)	53.6	[48]
Cu_2Te	Nowotny (<i>nw</i>)	117.5	mp-1861 [49]
Cu_2Te	Cường (<i>cg</i>)	0	[50]

^aA virtual expression of the ordered defect structure is used in DFT calculations.

^bParsimony condition (Pauling's fifth rule) fulfilled in cation ordering.

III. RESULTS AND DISCUSSION

The formation energies of all $(\text{Cu}_2\text{Te})_x(\text{In}_2\text{Te}_3)_{1-x}$ crystal structures considered in this study, including the pseudobinary terminus compositions Cu_2Te and In_2Te_3 , are summarized in Tables I and II and Fig. 2.

A. Cu_2Te and In_2Te_3

The position of the hull in the $(\text{Cu}_2\text{Te})_x(\text{In}_2\text{Te}_3)_{1-x}$ pseudobinary system is a cross section of the ternary hull of the Cu-In-Te system as depicted in Fig. 1(a). As such, it is partly dependent on the terminus compositions, indium telluride (In_2Te_3) and copper (I) telluride (Cu_2Te), as well as phases on the Cu-Te and In-Te binary systems [Fig. 1(b)].

In_2Te_3 , while not a hull material, has several observed phases. Most x-ray diffraction measurements discern a spha-

lerite (*Sp*) crystal structure in In_2Te_3 , with two possible crystal structure expressions from Zaslavskii *et al.* (Sp') [28] and Woolley *et al.* (Sp'') [29]; these are cross-evaluated in detail in Table III. In addition, a tellurobismuthite-type (*Tbi*) structure has been observed in high-pressure conditions [30]. Finally, we also include the distorted wurtzite structure (Wur') [32] of the closely related In_2Se_3 as a candidate structure for In_2Te_3 . All of these phases lie above the In-Te hull, and tend towards phase separation into $\text{In}_7\text{Te}_{10}$ and Te metal.

Cu_2Te is an interesting compound in its own right, owing to potential applications in thermoelectric devices and photocatalysis [52,53]. While the Nowotny structure [49] is the most commonly cited, materials discovery using high-throughput calculations has generated more phases of Cu_2Te more stable than the Nowotny structure in terms of formation energy. An earlier attempt by Da Silva *et al.* [54] found one

TABLE II. Description of defect-containing structures for DFT simulations. The sizes of the supercell used to accommodate defects in simulations are in terms of the tetragonal unit cell of CuInTe_2 [see Fig. 5(a)].

Defect ϕ	Description	Supercell	Defect concentration (10^{-1} nm^{-3})	$\Delta_H E_F$ (meV/atom)
afs'''	Dispersed $\text{Cu}_{\text{In}}^{2-}$ and Cu_i^+	$2 \times 2 \times 1$	5.3	17.3
cc	Corner-sharing $[\text{Cu}_{\text{In}} \cdot 2\text{Cu}_i]^0$	$2 \times 2 \times 1$	5.3	10.9
cec	Edge-sharing (cis) $[\text{Cu}_{\text{In}} \cdot 2\text{Cu}_i]^0$	$2 \times 2 \times 1$	5.3	5.5
cec	Edge-sharing (cis) $[\text{Cu}_{\text{In}} \cdot 2\text{Cu}_i]^0$	$2 \times 3 \times 1$	3.5	2.1
cet	Edge-sharing (trans) $[\text{Cu}_{\text{In}} \cdot 2\text{Cu}_i]^0$	$2 \times 2 \times 1$	5.3	5.4
cet	Edge-sharing (trans) $[\text{Cu}_{\text{In}} \cdot 2\text{Cu}_i]^0$	$2 \times 3 \times 1$	3.5	2.8
cet	Edge-sharing (trans) $[\text{Cu}_{\text{In}} \cdot 2\text{Cu}_i]^0$	$2 \times 2 \times 2$	2.7	1.7
cet	Edge-sharing (trans) $[\text{Cu}_{\text{In}} \cdot 2\text{Cu}_i]^0$	$3 \times 3 \times 2$	1.2	0.5

such phase which undercuts the Nowotny structure formation energy by 135 meV/atom, but failed to find any thermodynamically stable structure in relation to phase separation to Cu and Te. Later, Nguyen *et al.* [50] were able to find a layered phase of Cu_2Te (Cường phase, cg) through the adaptive genetic algorithm (AGA), which we find yields the lowest formation energy out of all the polymorphs analyzed and constitutes a vertex on the Cu-Te binary hull.

B. Search by mineral prototypes

Our initial approach to materials discovery in the Cu-In-Te ternary system is to collect existing crystal structures of chemically similar ternary systems as starting points for DFT structural optimization and formation energy calculations [Fig. 3(a)]. For Cu and Te sites, the criterion for similarity is isovalence, so substitutions of common elements (Cu, Ag in Cu sites; S, Se, and Te in Te sites) in the same group are considered. We consider common p -block metals and metalloids as substituted elements at the In sites. Indeed, many of the elements in groups 13–15 can adopt the cationic oxidation states +1 to +3, similar to In. To avoid encountering organic compounds, we exclude C, N, and O. Crystal structure

searches in Materials Project [12] and the Inorganic Crystal Structure Database (ICSD) [57] yield two unique structures with the 1:3:5 stoichiometry and three unique structures with the 5:1:4 stoichiometry.

Most compounds in the target stoichiometries, 1:3:5, 3:1:3, and 5:1:4, turn out large formation energies above the hull. The notable exception is the CuIn_3Se_5 -based structure (mp-1224175), which is metastable at only 6.7 meV/atom above the hull.

CuIn_3Se_5 -like CuIn_3Te_5 sits close to the hull because its crystal structure has an adamantine configuration, consisting of a network of corner-sharing InTe_4 and CuTe_4 tetrahedra. This also applies to the hull materials CuIn_5Te_8 (mp-1224528), as well as chalcopyrite CuInTe_2 (Ccp). Cu-In-Te compounds between CuIn_5Te_8 and CuInTe_2 have been experimentally determined to have defect-stabilized adamantine structures similar to chalcopyrite [3–9,58], including the defect stannite (Stn) crystal structure of the space group $I42m$ [9]. In fact, the structures from CuIn_5Te_8 (Stn') and CuIn_3Se_5 (Stn'') from the Materials Project database can be considered virtual expressions of the defect stannite structure [Fig. 3(c)].

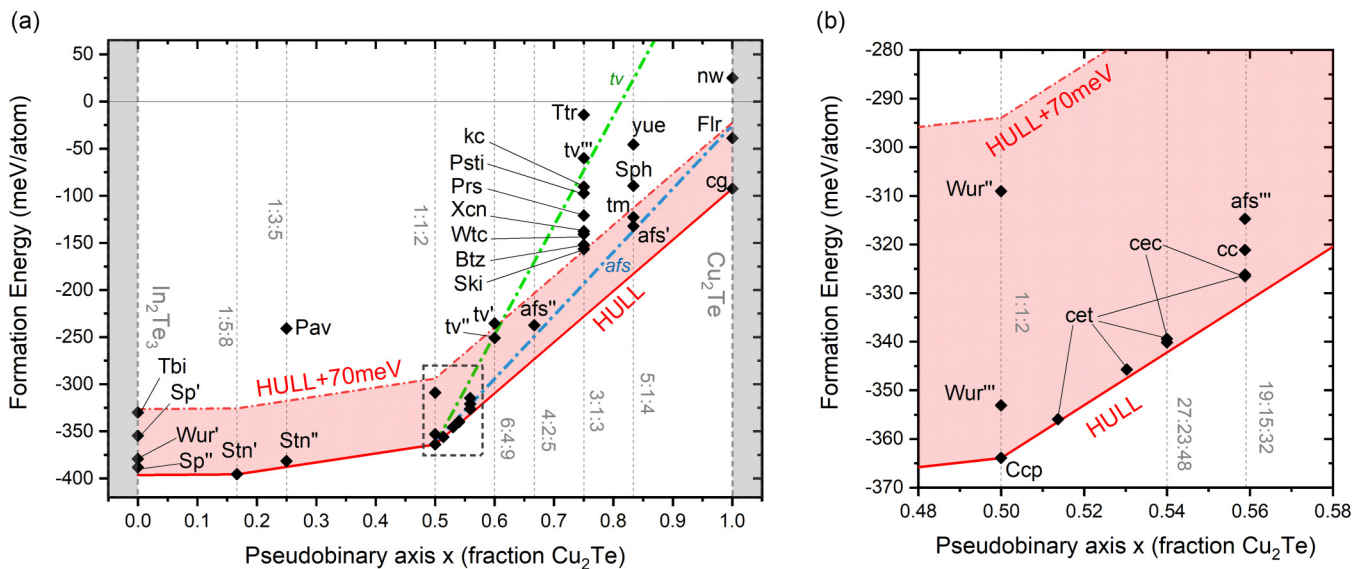


FIG. 2. Formation energy hull diagram of trial crystal structures of the $(\text{Cu}_2\text{Te})_x(\text{In}_2\text{Te}_3)_{1-x}$ pseudobinary system. Each point refers to a DFT-evaluated structure and is identified by its symbol (see Table I). A region of stability of up to 70 meV above the hull [51] is shown shaded in red. The antifluorite line (afs) and Te-vacancy line (tv) are also shown.

TABLE III. Importance of averageness in Te local coordination environments ($\bar{U}_{\text{Te} \rightarrow \text{In}}$, $\bar{U}_{\text{Te} \rightarrow \text{Cu}}$) in DFT stability. The set of coordination environments seen in a particular atomistic unit cell representation is compared against an average figure, showing an energy penalty for extreme values.

Phase ϕ	Te local coordination ($\bar{U}_{\text{Te} \rightarrow \text{In}}$, $\bar{U}_{\text{Te} \rightarrow \text{Cu}}$)		$\Delta_H E_F$ (meV/atom)
	Observed	Average	
<i>Ccp</i>	(2,2)	(2,2)	0
<i>Wur''</i>	(1,3) and (3,1)	(2,2)	54.9
<i>Wur'''</i>	(2,2)	(2,2)	10.8
<i>Sp'</i>	(0,0), (2,0), and (3,0)	($2\frac{2}{3}$,0)	41.6
<i>Sp''</i>	(2,0), (3,0)	($2\frac{2}{3}$,0)	8.0

In fact, the most negative formation energies are found for crystal structures with fourfold coordination on the Cu and In cation sites, in contrast to other coordination numbers. Figure 3(d) summarizes this for the terminus compounds and the mineral analogs, showing a distinct domain of adamantine structures with very negative formation energies, and mineral analogs with higher formation energies. Geometry optimization among 3:1:3 and 5:1:4 prototypes also increases the prevalence of fourfold-coordinated Cu sites from 25% to 55% and the prevalence of In sites from 9% to 32%. These are consistent with Pauling’s first rule for inorganic crystal structures, which states that cation/anion ratios determine the coordina-

tion tetrahedra [59]. Here, the cation/anion ratios $r_{\text{Cu}^+}/r_{\text{Te}^{2-}}$ and $r_{\text{In}^{3+}}/r_{\text{Te}^{2-}}$ are 0.348 and 0.361, respectively, favoring structures with predominantly tetrahedral coordination. Although the antiferite (*Flr*) and bytízite (*Btz*) structures are also predominantly fourfold coordinated, the energetic advantage from this property is negated by the fact that some adjacent CuTe_4 and InTe_4 tetrahedra are edge sharing instead of corner sharing, reflecting Pauling’s third rule [59], which states that corner-sharing tetrahedra are preferred over edge-sharing and face-sharing tetrahedra.

C. Search by construction

We now continue the search for the $(\text{Cu}_2\text{Te})_x(\text{In}_2\text{Te}_3)_{1-x}$ phase in the “augmented” regime ($x > 1/2$) in a more directed manner involving constructing DFT simulation cells dominated by fourfold-coordinated cation sites with defects introduced to arrive at a target stoichiometry. Two categories of crystal structures are constructed. First, quasiantiferite (*afs*) structures are constructed on the principle that only corner-sharing and edge-sharing tetrahedra are featured in the crystal structure, satisfying Pauling’s third rule [59]. Where the stoichiometry forces us to include atoms outside of the adamantine framework, we place exclusively Cu at tetrahedral sites outside of the adamantine framework. Second, Te-vacancy (*tv*) structures are constructed by creating Te-vacancies. The individual constructed structures are depicted in Fig. 4.

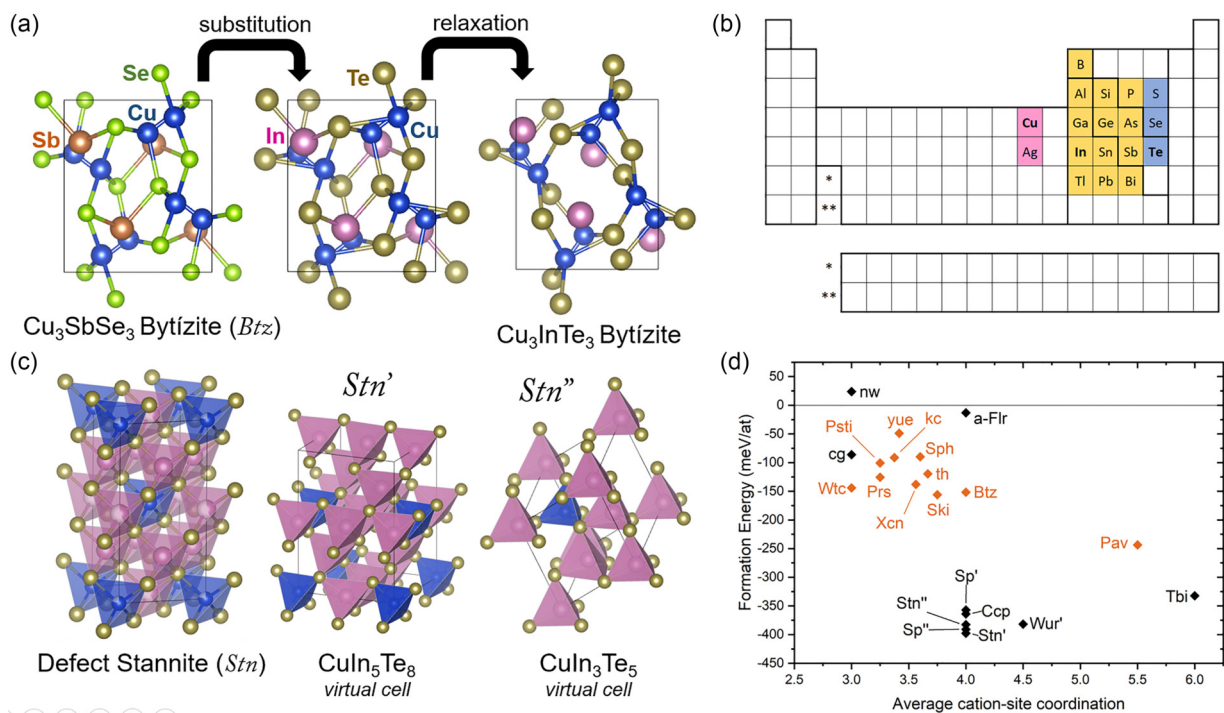


FIG. 3. (a) Process of adopting the crystal structure of a chemically similar mineral to the Cu-In-Te system, using the mineral bytízite (Cu_3SbSe_3) as an example. (b) Crystal structures are searched from ternary systems containing elements chemically similar to Cu (magenta), In (yellow), and Te (blue). (c) The defect stannite structure based on Refs. [9,55] and two of its virtual expressions found in the Materials Project database [12]. (d) Relationship between the average Te coordination number of Cu and In cation sites and the formation energy, with higher-energy mineral analog structure highlighted in orange (illustrations made with VESTA [56]).

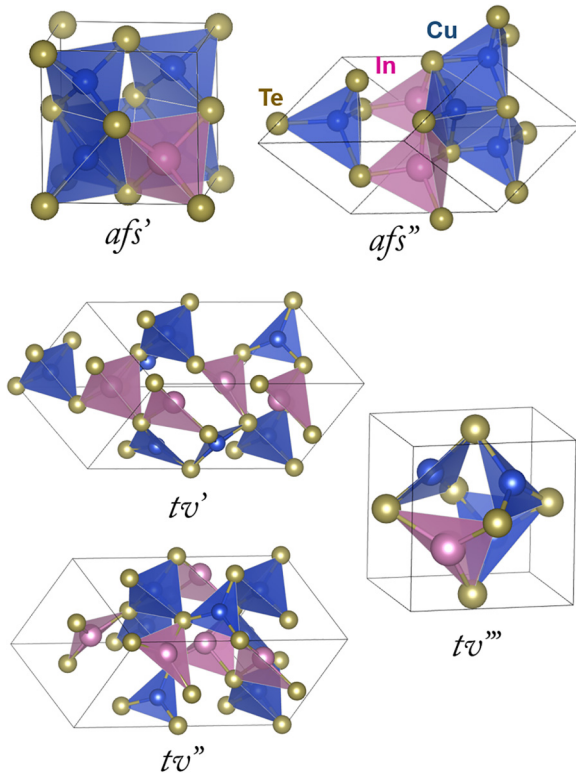


FIG. 4. Constructed virtual simulation cells including quasiauto-fluorite structures (*afs*) and tellurium-vacancy structures (*tv*) (illustrations made with VESTA [56]).

These two categories of constructed crystals are shown to exhibit consistent linear trends in formation energy in the augmented regime, as shown in Fig. 2(a) with lines labeled *afs* and *tv*. The formation energy of *tv* structures is shown to be higher than *afs* structures for the same value of x . Featureally, the origin of this difference becomes clear when considering that the creation of one V_{Te} defect concurrently creates four trigonal-pyramidal-coordinated cation sites around it, which sometimes transform into trigonal-planar-coordinated cations upon structural relaxation. (The extreme case is tv''' , which is made up exclusively of trigonal-planar-coordinated cations.) By violating Pauling's first rule, *tv* structures incur a larger energy penalty than *afs* structures.

D. Defect cluster-containing structures

The linear trend in formation energy over composition for *afs*-type crystal structures suggests, at the region where $x > 1/2$ in the $(\text{Cu}_2\text{Te})_x(\text{In}_2\text{Te}_3)_{1-x}$ pseudobinary system, that *afs*-type crystal structures would approach the hull as x approaches 1/2. In this regime, stoichiometry is maintained through the creation of $\text{Cu}_{\text{In}}^{2-}$ substitutional and Cu_i^+ interstitial defects; this mirrors the formation of V_{Cu}^- and $\text{In}_{\text{Cu}}^{2+}$ defects in defect chalcopyrites [6]. To study this in detail, it is necessary to create a supercell of tetragonal chalcopyrite unit cells to ensure sufficient distance between defects in neighboring periodic images. Next, a number of configurations of point-defect distributions are evaluated using geometric optimization, where the positions of all atoms are allowed to relax

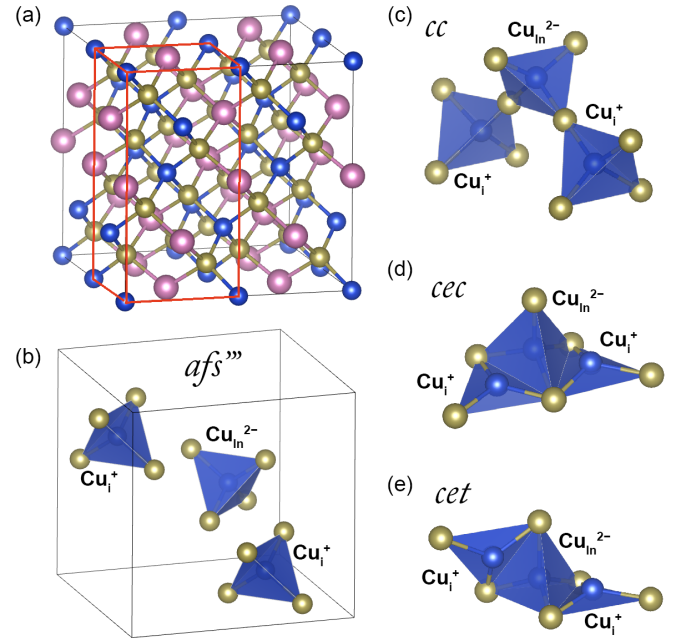


FIG. 5. Construction of defect-containing supercells of chalcopyrite CuInTe_2 of various clustering configurations. (a) Construction of a $2 \times 2 \times 1$ supercell from one tetragonal unit cell of CuInTe_2 (highlighted with red lines). (b) A unit cell of $\text{Cu}_{19}\text{In}_{15}\text{Te}_{32}$ (*afs'''*) featuring the stoichiometry-maintaining defects in a disperse configuration. [(c)–(e)] $[\text{Cu}_{\text{In}} \cdot 2\text{Cu}_i]^0$ defect clusters in corner-sharing (*cc*), edge-sharing cis (*cec*), and edge-sharing trans (*cet*) configurations (illustrations made with VESTA [56]).

to the lowest-energy configurations, and subsequently total energy calculations. These are described and summarized in Fig. 5 and Table II.

The difference between stoichiometry-maintaining defects being in a disperse configuration and being bounded in a defect cluster is evident from the energy difference between *afs'''* and *cc* (6.4 meV/atom) and between *afs'''* and *cec* (11.8 meV/atom). This follows from the fact that the point defects $\text{Cu}_{\text{In}}^{2-}$ and Cu_i^+ bear opposite charges, and can attract each other to be bound in a quasimolecule in the *Ccp* crystalline matrix during synthesis. The larger energy release in creating a *cec* defect cluster as compared to a *cc* defect cluster is due to the fact that the opposite-charged cation sites are much closer in *cc* (2.3 Å) than in *cec* (5.2 Å). This is in apparent violation of Pauling's third rule, but consistent with electrostatics.

To split hairs further, two configurations are possible in the edge-sharing defect cluster: the cis configuration (*cec*), where two Cu_i^+ share adjacent edges on the $\text{Cu}_{\text{In}}^{2-}$ tetrahedron, and the trans configuration (*cet*), where two Cu_i^+ share opposite edges from each other on the $\text{Cu}_{\text{In}}^{2-}$ tetrahedron. Between them, the trans configuration separates the two positively charged Cu_i^+ sites by 4.7 Å, 0.5 Å more than the cis configuration. The Cu_i^+ sites are pulled inwards sufficiently during geometric optimization to assume a planar trigonal coordination to their nearest-neighboring Te sites instead of the projected tetrahedral coordination. However, the energy difference between the cis and trans configurations is negligible, on the order of less than 1 meV per defect.

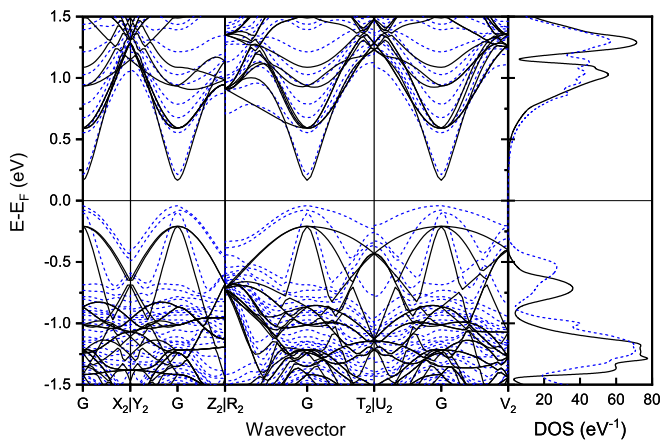


FIG. 6. Band structure and density of states (DOS) of a $2 \times 2 \times 1$ CuInTe₂ supercell, pristine (black solid lines) or with a *cec* defect (blue dashed lines).

Figure 2(b) and Table II show that the more dilute the *cec* defects present in a *Ccp* crystal structure, the lower the formation energy of the cell. This is achieved by enlarging the size of the *Ccp* supercell which would accommodate one *cec* defect cluster. The lowest concentration we have calculated has one *cec* defect cluster per 18 tetragonal *Ccp* unit cells, corresponding to 72 formula units of CuInTe₂. This concentration yields a formation energy of only 0.5 meV above hull.

For a clearer picture on the influence of a defect cluster on the electronic structure of CuInTe₂, we studied the influence of a *cec* defect in a $2 \times 2 \times 1$ CuInTe₂ supercell, which is visualized in Fig. 6. The corresponding defect occupancy relative to the total number of In sites is 6.25%, and the corresponding defect concentration is 0.53 units/nm³. Our GGA+*U* calculations determine the band gap of CuInTe₂ at 0.38 eV, smaller than the experimental value of ≈ 1.1 eV [34,60] (in comparison, the removal of the Hubbard *U* parameter leads to the prediction of a zero-band-gap material).

Here, we must note that methods involving GGA+*U* are optimized for thermochemistry applications, rather than accurate band-structure predictions. The result is that the band gaps of semiconductors and insulators tend to be underestimated, as in pure DFT. (In the case of CuInTe₂, the underestimation persists even with more advanced Heyd-Scuzeria-Ernzerhof hybrid functionals and taking spin-orbit coupling into account, producing a band gap of 0.54 eV [61].) The inclusion of a *cec* defect is found to increase the energy of the conduction-band minimum by ≈ 0.05 eV and to increase the energy of the valence-band maximum by ≈ 0.17 eV, resulting in a net band-gap narrowing of ≈ 0.12 eV.

E. Parsimony condition

A crystal structure property which has a strong influence in DFT-calculated formation energies would be the coordination environment of the anion Te²⁻. In the (Cu₂Te)_{*x*}(In₂Te₃)_{1-*x*} system, Te²⁻ sites are coordinated with Cu⁺ and/or In³⁺. Our calculations on various phases suggest that Pauling's fifth rule, also called the rule of parsimony, has a significant influence on formation energy.

The rule of parsimony states that the number of distinct constituents in an ionic crystal tends to be small, so that local concentrations of electric charge are minimized as much as possible. This manifests in two particular tendencies in relation to Te sites. First, all Te sites in the crystal structure tend towards the same coordination environment. For crystal structures dominated by a corner-sharing tetrahedral network, this means that each Te tends to be coordinated to the same set of In or Cu sites, including partially occupied sites.

Second, the Te coordination environment favors fully occupied In or Cu sites over partially occupied sites. For example, if a Te site is coordinated to 8/3 In on average ($\bar{U}_{\text{Te} \rightarrow \text{In}} = 8/3$), as is the case for In₂Te₃, this manifests as a coordination to two fully occupied In sites and one 1/3-occupied In site, rather than as a coordination to four partially occupied In sites. If this were not the case, compounding probabilities would result in a nonzero probability of an energetically costly Te coordination of 4 or of 0. Thus, by the criterion of average-ness, a virtual In₂Te₃ DFT cell should contain Te sites with coordination strictly between 2 and 3.

To reflect the correlation between parsimony in local coordination environments and the formation energy, we make an example of two sets of structures based on wurtzite (*Wur*) and sphalerite (*Sp*). The comparison is shown in Table III.

Based on stoichiometry, the average coordination numbers $\bar{U}_{\text{Te} \rightarrow \text{Cu}}$ and $\bar{U}_{\text{Te} \rightarrow \text{In}}$ are both 2 in CuInTe₂. We know this to hold true in the hull (*Ccp*) structure.

While *Wur''* has a mix of Te sites of coordinations $\bar{U}_{\text{Te} \rightarrow \text{Cu}} = 1$ and $\bar{U}_{\text{Te} \rightarrow \text{In}} = 3$ and Te sites of coordinations $\bar{U}_{\text{Te} \rightarrow \text{Cu}} = 3$ and $\bar{U}_{\text{Te} \rightarrow \text{In}} = 1$, *Wur'''* only has Te sites of coordinations $\bar{U}_{\text{Te} \rightarrow \text{Cu}} = 2$ and $\bar{U}_{\text{Te} \rightarrow \text{In}} = 2$, in a more average configuration, similar to *Ccp*. This results in the lower formation energy of *Wur'''* with an energy difference of 44.1 meV/atom compared to *Wur''*. In contrast, the formation energy difference between *Wur'''* and *Ccp* is only 10.8 meV/atom, despite being of a completely different crystal system.

We can also see the effects of parsimony in two expressions of sphalerite-type (*Sp*) In₂Te₃ from the Materials Project database [12]. The first (mp-622511, *Sp'*) is identical to the *F*43*m* structure observed by Zaslavskii *et al.* [28]. The second (mp-1223866, *Sp''*) is based on a different proposed interpretation of the x-ray diffraction data by Woolley *et al.* [29]. Both are built with a face-centered-cubic ordering of Te sites, with differences in the ordering of In sites.

A closer look into *Sp'* structure reveals the presence of four Te atoms which are not coordinated to any In. In contrast, *Sp''* contains a 2:1 mix of three-coordinated Te and two-coordinated Te sites in a virtual cell. By having Te coordinated to strictly two or three In sites, *Sp''* conforms to Pauling's rule of parsimony much better than *Sp'*. This is reflected in the lower formation energy of *Sp''*, with the energy difference of 33.6 meV/atom compared to *Sp'*.

In reality, the tendency to parsimony is reflected in the Cu₃In₅Te₉ cell of Guedez *et al.* [9] and the CuIn₃Se₅ cell of Hanada *et al.* [55] (Fig. 7), both ordered vacancy crystal structures where each Te atom is coordinated to the same set of fully or partially occupied Cu and In sites which at the same time are as filled as possible, given the stoichiometry. The condition that each Te atom tends to see the same coordination

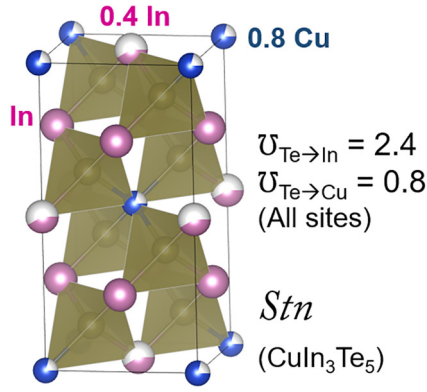


FIG. 7. A unit cell of CuIn_3Te_5 of the defect stannite symmetry (*Stn*) based on Ref. [55], showing Te-centered coordination polyhedra (illustration made with VESTA [56]).

environment is thus satisfied. In this way, the relationship between formation energy and Pauling's rule of parsimony explains the prevalence of ordered vacancy structures in the $x < 1/2$ regime of our pseudobinary system.

F. Hybridization effects

The question now would be to ask whether adamantine structure can be found throughout the $(\text{Cu}_2\text{Te})_x(\text{In}_2\text{Te}_3)_{1-x}$ pseudobinary system. Assuming an adamantine tetrahedral network $(\text{Cu}_2\text{Te})_x(\text{In}_2\text{Te}_3)_{1-x}$ with face-centered-cubic arrangement of Te sites, the coordination of the Te atom is governed by the stoichiometry of the compound. Expanding the formula $(\text{Cu}_2\text{Te})_x(\text{In}_2\text{Te}_3)_{1-x}$ and visualizing that a cation site is shared by the four coordinating Te sites, we obtain the equation

$$\begin{aligned} \bar{U}_{\text{Te}}(x) &= \bar{U}_{\text{Te} \rightarrow \text{Cu}}(x) + \bar{U}_{\text{Te} \rightarrow \text{In}}(x) \\ &= \frac{8x}{3-2x} + \frac{8-8x}{3-2x} = \frac{8}{3-2x}. \end{aligned} \quad (2)$$

Plotting these equations in the same graph and extrapolating to $x > 1/2$, we arrive at Fig. 8.

Indeed, $\bar{U}_{\text{Te} \rightarrow \text{In}}(0) = 8/3$, which is the case for In_2Te_3 , and $\bar{U}_{\text{Te} \rightarrow \text{Cu}}(1) = 8$, which is the case for antifluorite Cu_2Te , and $\bar{U}_{\text{Te} \rightarrow \text{Cu}}(1/2) = \bar{U}_{\text{Te} \rightarrow \text{In}}(1/2) = 2$, which is the case of chalcopyrite CuInTe_2 .

For $x = 5/6$, Te-coordination \bar{U}_{Te} sits at 6, which is the coordination seen in most of the naturally occurring and predicted phases of Cu_2Te , such as the Cường phase (*cg*) [50] and rickardite [62]. Beyond this point, phases built in the adamantine motif, such as antifluorite (*Flr*), will become unstable [48]. A likely reason for this is that the six-coordinated Te engages all six Te 5*p* states in interatomic bonding. This configuration completely hybridizes all Te 5*p* orbitals. Te coordinations beyond six would imply that less than one electron on average is allocated to a Te-metal bond, which contributes to instability.

On a related note, Cu_2Te phases themselves tend towards layered rather than bulk structures [49,50,54,63] and exhibit a tendency to Cu deficiency in stoichiometry [62,64–66]. Both

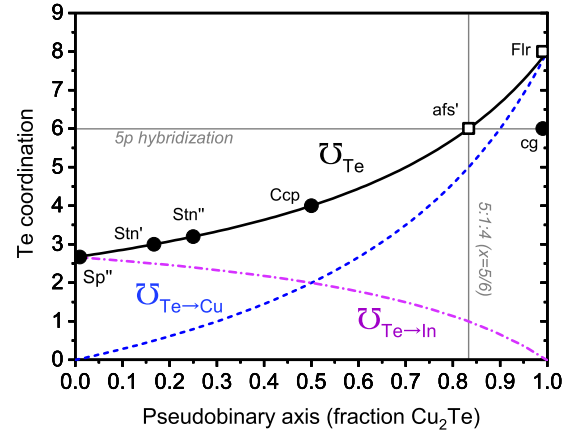


FIG. 8. Te coordination parameters described in Eq. (2) in the pseudobinary space of $(\text{Cu}_2\text{Te})_x(\text{In}_2\text{Te}_3)_{1-x}$, according to the adamantine motif. Some of the near-hull phases (black circles) and higher-energy phases (white squares) are shown. A stable structure in the range $x > 5/6$ should detract from the adamantine motif, as exemplified by the Cường phase (*cg*).

layered phases and Cu deficiency serve to limit the Te coordination numbers $\bar{U}_{\text{Te} \rightarrow \text{Cu}}$ to six or fewer.

IV. CONCLUSION

The main conclusion of this work is the existence of the augmented chalcopyrite, which can be thought of as a sister class of the defect chalcopyrite, except that the defects in question come in the form of the charge-compensated defect cluster $[\text{Cu}_{\text{In}} \cdot 2\text{Cu}_i]^0$ of Cu interstitial and substitutional defects instead of vacancies. We show that, by the criterion of formation energy above hull, a small regime on the Cu-rich side of the $(\text{Cu}_2\text{Te})_x(\text{In}_2\text{Te}_3)_{1-x}$ pseudobinary system exhibits very low formation energies above the hull and can be considered to be stable. The elevated Cu_2Te content narrows the band gap, providing an avenue of band-gap tunability by chemical composition.

More significantly, DFT calculations on various fictitious materials reveal the strong dependence of the predicted formation energy on local coordination environments and a preference for crystal structures adhering to Pauling's rules for ionic solids in the $(\text{Cu}_2\text{Te})_x(\text{In}_2\text{Te}_3)_{1-x}$ pseudobinary system. In contrast, the mineral prototype method for the search of polymorphic phases has largely failed to predict stable phases in this system, due to the lack of perspective of Pauling's rules.

The limitations of the predictive power of Pauling's rules have been noted by George *et al.* [67], based on the ability of Pauling's rules to predict experimentally attested phases. Nevertheless, they work well in explaining the large DFT energy differences between fictitious phases. Where conflicting interpretations of x-ray diffraction data exist, as in In_2Te_3 and CuIn_3Te_5 , Pauling's fifth rule can provide a perspective on which interpretation is the most reasonable.

A possible systematized predictor of stability of ionic and covalently bonded multielemental systems can be based primarily on the local coordination environment. The challenge, going forward, is whether a complete crystal structure can be derived solely based on local coordination environments.

Finally, one must recognize that the fabrication of predicted near-hull phases may not necessarily be trivial. A case in point would be the hull structure of Cu_2Te according to Nguyen *et al.* [50] which, even while it is predicted to have a low formation energy and to be stable by phonon calculations, has not been observed in experiment for two decades since its prediction.

ACKNOWLEDGMENTS

K.H. acknowledges funding from the Singapore National Research Foundation (NRF) Fellowship No. NRF-NRFF13-2021-0011, and the Agence Nationale de la Recherche - National Research Foundation (ANR-NRF) joint collaboration Project No. NRF2020-NRF-ANR104 DesperQD.

- [1] Y. Cao, X. Su, F. Meng, T. P. Bailey, J. Zhao, H. Xie, J. He, C. Uher, and X. Tang, Origin of the distinct thermoelectric transport properties of chalcopyrite ABTe_2 ($A = \text{Cu}, \text{Ag}$; $B = \text{Ga}, \text{In}$), *Adv. Funct. Mater.* **30**, 2005861 (2020).
- [2] J. M. Adamczyk, L. C. Gomes, J. Qu, G. A. Rome, S. M. Baumann, E. Ertekin, and E. S. Toberer, Native defect engineering in CuInTe_2 , *Chem. Mater.* **33**, 359 (2021).
- [3] E. M. Kadykalo, L. P. Marushko, I. A. Ivashchenko, O. F. Zmiy, and I. D. Olekseyuk, Quasi-ternary system $\text{Cu}_2\text{Te}-\text{CdTe}-\text{In}_2\text{Te}_3$, *J. Phase Equilib. Diffus.* **34**, 221 (2013).
- [4] D. Ni, L. T. Nguyen, E. S. Feverston, R. Zhong, and R. J. Cava, High resolution structural refinement and band gap characterization of the defect chalcopyrites CuIn_5Te_8 , AgIn_5Te_8 and AuIn_5Te_8 , *J. Solid State Chem.* **292**, 121752 (2020).
- [5] C. Rincón, S. M. Wasim, G. Marín, E. Hernández, J. M. Delgado, and J. Galibert, Raman spectra of CuInTe_2 , CuIn_3Te_5 , and CuIn_5Te_8 ternary compounds, *J. Appl. Phys.* **88**, 3439 (2000).
- [6] C. Rincón, S. M. Wasim, G. Marín, J. M. Delgado, and J. Contreras, Effect of ordered arrays of native defects on the crystal structure of In- and Ga-rich Cu-ternaries, *Appl. Phys. Lett.* **83**, 1328 (2003).
- [7] R. Díaz, L. Bisson, F. Agulló-Rueda, M. A. Lefdil, and F. Rueda, Effect of composition gradient on CuIn_3Te_5 single-crystal properties and micro-Raman and infrared spectroscopies, *Appl. Phys. A* **81**, 433 (2005).
- [8] T. Plirdpring, K. Kurosaki, A. Kosuga, M. Ishimaru, Y. Ohishi, H. Muta, and S. Yamanaka, High-temperature thermoelectric properties of $\text{Cu}_2\text{In}_4\text{Te}_7$, *Phys. Status Solidi RRL* **6**, 154 (2012).
- [9] E. Guedez, L. Mogollón, G. Marcano, S. Wasim, G. Sánchez Pérez, and C. Rincón, Structural characterization and optical absorption spectrum of $\text{Cu}_3\text{In}_5\text{Te}_9$ ordered defect semiconducting compound, *Mater. Lett.* **186**, 155 (2017).
- [10] J. E. Bernard and A. Zunger, Ordered-vacancy-compound semiconductors: Pseudocubic CdIn_2Se_4 , *Phys. Rev. B* **37**, 6835 (1988).
- [11] C. Toher, C. Oses, D. Hicks, and S. Curtarolo, Unavoidable disorder and entropy in multi-component systems, *npj Comput. Mater.* **5**, 69 (2019).
- [12] A. Jain, S. P. Ong, G. Hautier, W. Chen, W. D. Richards, S. Dacek, S. Cholia, D. Gunter, D. Skinner, G. Ceder, and K. A. Persson, Commentary: The Materials Project: A materials genome approach to accelerating materials innovation, *APL Mater.* **1**, 011002 (2013).
- [13] S. Kirklin, J. E. Saal, B. Meredig, A. Thompson, J. W. Doak, M. Aykol, S. Rühl, and C. Wolverton, The Open Quantum Materials Database (OQMD): Assessing the accuracy of DFT formation energies, *npj Comput. Mater.* **1**, 15010 (2015).
- [14] A. Lee, S. Sarker, J. Saal, L. Ward, C. Borg, A. Mehta, and C. Wolverton, Machine learned synthesizability predictions aided by density functional theory, *Commun. Mater.* **3**, 73 (2022).
- [15] L. N. Warr, IMA-CNMNC approved mineral symbols, *Mineral. Mag.* **85**, 291 (2021).
- [16] G. Kresse and J. Hafner, *Ab initio* molecular dynamics for liquid metals, *Phys. Rev. B* **47**, 558(R) (1993).
- [17] G. Kresse and J. Hafner, *Ab initio* molecular-dynamics simulation of the liquid-metal-amorphous-semiconductor transition in germanium, *Phys. Rev. B* **49**, 14251 (1994).
- [18] G. Kresse and J. Furthmüller, Efficiency of ab-initio total energy calculations for metals and semiconductors using a plane-wave basis set, *Comput. Mater. Sci.* **6**, 15 (1996).
- [19] G. Kresse and J. Furthmüller, Efficient iterative schemes for *ab initio* total-energy calculations using a plane-wave basis set, *Phys. Rev. B* **54**, 11169 (1996).
- [20] J. P. Perdew, K. Burke, and M. Ernzerhof, Generalized gradient approximation made simple, *Phys. Rev. Lett.* **77**, 3865 (1996).
- [21] J. P. Perdew, K. Burke, and M. Ernzerhof, Erratum: Generalized gradient approximation made simple [Phys. Rev. Lett. **77**, 3865 (1996)], *Phys. Rev. Lett.* **78**, 1396(E) (1997).
- [22] V. I. Anisimov, J. Zaanen, and O. K. Andersen, Band theory and Mott insulators: Hubbard U instead of Stoner I , *Phys. Rev. B* **44**, 943 (1991).
- [23] B. Himmetoglu, A. Floris, S. De Gironcoli, and M. Cococcioni, Hubbard-corrected DFT energy functionals: The LDA+ U description of correlated systems, *Int. J. Quantum Chem.* **114**, 14 (2014).
- [24] S. L. Dudarev, G. A. Botton, S. Y. Savrasov, C. J. Humphreys, and A. P. Sutton, Electron-energy-loss spectra and the structural stability of nickel oxide: An LSDA+ U study, *Phys. Rev. B* **57**, 1505 (1998).
- [25] A. Jain, G. Hautier, S. P. Ong, C. J. Moore, C. C. Fischer, K. A. Persson, and G. Ceder, Formation enthalpies by mixing GGA and GGA+ U calculations, *Phys. Rev. B* **84**, 045115 (2011).
- [26] A. A. Emery and C. Wolverton, High-throughput DFT calculations of formation energy, stability and oxygen vacancy formation energy of ABO_3 perovskites, *Sci. Data* **4**, 170153 (2017).
- [27] V. Stevanović, S. Lany, X. Zhang, and A. Zunger, Correcting density functional theory for accurate predictions of compound enthalpies of formation: Fitted elemental-phase reference energies, *Phys. Rev. B* **85**, 115104 (2012).
- [28] A. I. Zaslavskii, V. M. Sergeeva, and A. I. Smirnov, The polymorphism of In_2Te_3 , *Sov. Phys. Solid State (New York)* **2**, 2556 (1960).
- [29] J. C. Woolley, B. R. Pamplin, and P. J. Holmes, The ordered crystal structure of In_2Te_3 , *J. Less-Common Met.* **1**, 362 (1959).

- [30] S. Geller, A. Jayaraman, and G. W. Hull, Jr., Crystal chemistry and superconductivity of pressure-induced phases in the In-Te system, *J. Phys. Chem. Solids* **26**, 353 (1965).
- [31] N. Serebryanaya, The crystal structure of pressure-induced phases of In_2Te_3 and Ga_2Te_3 , *Powder Diffr.* **7**, 99 (1992).
- [32] A. Likforman, D. Carré, and R. Hillel, Structure cristalline du séléniure d'indium In_2Se_3 , *Acta Cryst. Sect. B* **34**, 1 (1978).
- [33] J.-H. Kim, D.-Y. Chung, D. Bilc, S. Loo, J. Short, S. D. Mahanti, T. Hogan, and M. G. Kanatzidis, Crystal growth, thermoelectric properties, and electronic structure of AgBi_3S_5 and $\text{AgSb}_x\text{Bi}_{3-x}\text{S}_5$ ($x = 0.3$), *Chem. Mater.* **17**, 3606 (2005).
- [34] M. V. Yakushev, A. V. Mudryi, E. Kärber, P. R. Edwards, and R. W. Martin, The band structure of CuInTe_2 studied by optical reflectivity, *Appl. Phys. Lett.* **114**, 062103 (2019).
- [35] K. S. Knight, The crystal structures of CuInSe_2 and CuInTe_2 , *Mater. Res. Bull.* **27**, 161 (1992).
- [36] R. Liu, L. Xi, H. Liu, X. Shi, W. Zhang, and L. Chen, Ternary compound CuInTe_2 : A promising thermoelectric material with diamond-like structure, *Chem. Commun.* **48**, 3818 (2012).
- [37] B. J. Wuensch, The crystal structure of tetrahedrite, $\text{Cu}_{12}\text{Sb}_4\text{S}_{13}$, *Z. Kristallogr.* **119**, 437 (1964).
- [38] P. Škácha, J. Sejkora, and J. Plášil, Bytízite, a new Cu-Sb selenide from Příbram, Czech Republic, *Mineral. Mag.* **82**, 199 (2018).
- [39] V. Kocman and E. W. Nuffield, The crystal structure of wittenite, Cu_3BiS_3 , *Acta Cryst. Sect. B* **29**, 2528 (1973).
- [40] A. Pfitzner, Cu_3SbS_3 : Zur Kristallstruktur und Polymorphie, *Z. Anorg. Allg. Chem.* **620**, 1992 (1994).
- [41] E. Makovicky and T. Balić-Žunić, The crystal structure of skinnerite, $P21/c$ - Cu_3SbS_3 , from powder data, *Can. Mineral.* **33**, 655 (1995).
- [42] D. Harker, The application of the three-dimensional Patterson method and the crystal structures of proustite, Ag_3AsS_3 , and pyrargyrite, Ag_3SbS_3 , *J. Chem. Phys.* **4**, 381 (1936).
- [43] C. Biagioni, F. Zaccarini, P. Roth, and L. Bindi, Progress in the knowledge of 'ruby silvers': New structural and chemical data of pyrostilpnite, Ag_3SbS_3 , *Mineral. Mag.* **84**, 463 (2020).
- [44] P. Engel and W. Nowacki, Die Kristallstruktur von Xanthokon, Ag_3AsS_3 , *Acta Cryst. Sect. B* **24**, 77 (1968).
- [45] M. G. Kanatzidis and J.-H. Chou, Isolation of β - Ag_3AsSe_3 , $(\text{Me}_3\text{NH})[\text{Ag}_3\text{As}_2\text{Se}_5]$, $\text{K}_5\text{Ag}_2\text{As}_3\text{Se}_9$, and $\text{KAg}_3\text{As}_2\text{S}_5$: Novel solid state silver thio- and selenoarsenates from solventothermal synthesis, *J. Solid State Chem.* **127**, 186 (1996).
- [46] D. J. Thomas, Analogie structurale des combinaisons sulfurées contenant du bore ou du cilicium et du cuivre ou de l'argent, *C. R. Acad. Sci. Paris Ser. C* **265**, 1325 (1967).
- [47] C.-Y. Yue, H.-P. Zhang, X.-X. Lu, Y.-Q. Bai, H. Shi, and X. Xu, Solvothermal syntheses and characterizations of two new silver selenidoantimonates of Ag_3SbSe_3 and Ag_5SbSe_4 , *Chin. J. Struct. Chem.* **35**, 227 (2016).
- [48] Y. Zhang, Y. Wang, L. Xi, R. Qiu, X. Shi, P. Zhang, and W. Zhang, Electronic structure of antiferroite Cu_2X ($\text{X} = \text{S}, \text{Se}, \text{Te}$) within the modified Becke-Johnson potential plus an on-site Coulomb U , *J. Chem. Phys.* **140**, 074702 (2014).
- [49] H. Nowotny, Die Kristallstruktur von Cu_2Te , *Int. J. Mater. Res.* **37**, 40 (1946).
- [50] M. C. Nguyen, J. H. Choi, X. Zhao, C. Z. Wang, Z. Zhang, and K. M. Ho, New layered structures of cuprous chalcogenides as thin film solar cell materials: Cu_2Te and Cu_2Se , *Phys. Rev. Lett.* **111**, 165502 (2013).
- [51] W. Sun, A. Holder, B. Orvañanos, E. Arca, A. Zakutayev, S. Lany, and G. Ceder, Thermodynamic routes to novel metastable nitrogen-rich nitrides, *Chem. Mater.* **29**, 6936 (2017).
- [52] Y. He, T. Zhang, X. Shi, S.-H. Wei, and L. Chen, High thermoelectric performance in copper telluride, *NPG Asia Mater.* **7**, e210 (2015).
- [53] D. J. Lee, G. Mohan Kumar, V. Ganesh, H. C. Jeon, D. Y. Kim, T. W. Kang, and P. Ilanchezhian, Novel nanoarchitectured Cu_2Te as a photocathodes for photoelectrochemical water splitting applications, *Nanomaterials* **12**, 3192 (2022).
- [54] J. L. Da Silva, S. H. Wei, J. Zhou, and X. Wu, Stability and electronic structures of Cu_xTe , *Appl. Phys. Lett.* **91**, 091902 (2007).
- [55] T. Hanada, A. Yamana, Y. Nakamura, O. Nittono, and T. Wada, Crystal structure of CuIn_3Se_5 semiconductor studied using electron and x-ray diffractions, *Jpn. J. Appl. Phys.* **36**, L1494 (1997).
- [56] K. Momma and F. Izumi, VESTA 3 for three-dimensional visualization of crystal, volumetric and morphology data, *J. Appl. Cryst.* **44**, 1272 (2011).
- [57] G. Bergerhoff, R. Hundt, R. Sievers, and I. D. Brown, The inorganic crystal structure data base, *J. Chem. Inf. Comput. Sci.* **23**, 66 (1983).
- [58] S. B. Zhang, S.-H. Wei, A. Zunger, and H. Katayama-Yoshida, Defect physics of the CuInSe_2 chalcopyrite semiconductor, *Phys. Rev. B* **57**, 9642 (1998).
- [59] L. Pauling, The principles determining the structure of complex ionic crystals, *J. Am. Chem. Soc.* **51**, 1010 (1929).
- [60] G. Jia and J. Du, Solution-liquid-solid growth of CuInTe_2 and $\text{CuInSe}_x\text{Te}_{2-x}$ semiconductor nanowires, *Inorg. Chem.* **57**, 14961 (2018).
- [61] K. Inzani, A. Faghaninia, and S. M. Griffin, Prediction of tunable spin-orbit gapped materials for dark matter detection, *Phys. Rev. Res.* **3**, 013069 (2021).
- [62] S. A. Forman and M. A. Peacock, Crystal structure of rickardite, $\text{Cu}_{4-x}\text{Te}_2$, *Am. Mineral.* **34**, 441 (1949).
- [63] Y. Tong, M. Bouaziz, W. Zhang, B. Obeid, A. Loncle, H. Oughaddou, H. Enriquez, K. Chaouchi, V. Esaulov, Z. Chen, H. Xiong, Y. Cheng, and A. Bendounan, Evidence of new 2D material: Cu_2Te , *2D Mater.* **7**, 035010 (2020).
- [64] Yu. G. Asadov, L. V. Rustamova, G. B. Gasimov, K. M. Jafarov, and A. G. Babajev, Structural phase transitions in Cu_{2-x}Te crystals ($x = 0.00, 0.10, 0.15, 0.20, 0.25$), *Phase Trans.* **38**, 247 (1992).
- [65] I. R. Amiraslanov, N. A. Alieva, G. G. Guseinov, and G. M. Agamirzoeva, Crystal structure of Cu_{2-m}Te ($m = 0.25$), *Cryst. Rep.* **62**, 210 (2017).
- [66] S. Liu, W. Xia, K. Huang, D. Pei, T. Deng, A. J. Liang, J. Jiang, H. F. Yang, J. Zhang, H. J. Zheng, Y. J. Chen, L. X. Yang, Y. F. Guo, M. X. Wang, Z. K. Liu, and Y. L. Chen, Measurement of electronic structure and surface reconstruction in the superionic Cu_{2-x}Te , *Phys. Rev. B* **103**, 115127 (2021).
- [67] J. George, D. Waroquiers, D. Di Stefano, G. Petretto, G. Rignanes, and G. Hautier, The limited predictive power of the Pauling rules, *Angew. Chem. Int. Ed.* **59**, 7569 (2020).